humanized mice (fig. S9). The frequency of HIV-1_{YU2}–infected cells before treatment was comparable in all groups of mice (fig. S10). As expected, mice treated with the Fc mutant antibody GRLR-3BNC117, which neutralizes HIV-1 but does not interact with effector cells, had lower frequencies of infected cells compared with isotype-treated controls (P = 0.0219) (Fig. 3D). However, mice treated with wild-type 3BNC117, which can mediate ADCC and ADCP, had substantially fewer infected cells compared with mice treated with GRLR-3BNC117 (P = 0.0167) (Fig. 3D). These data suggest that 3BNC117 can accelerate clearance of HIV-1_{YU2}–infected cells in the context of chronic viral infection.

In contrast to ART, antibodies have the potential to engage host immune cells in defense against the virus. They do so by binding to cell-free virions, which accelerates clearance and prevents their entry into target cells. Antibodies can also bind to HIV-1 Env on the surface of infected cells to induce ADCC or phagocytosis. Finally, immune complexes can activate antigen-presenting dendritic cells to elicit adaptive immune responses (*19*).

Both neutralizing and non-neutralizing antibodies support anti–HIV-1 ADCC activity in vitro (*5*, *21*), and Fc receptor binding is essential for optimal protection, postexposure prophylaxis, and therapy by bNAbs in animal models (*17*, *18*, *22*–*24*). Moreover, ADCC has been indirectly associated with both control of and protection against infection (*15*, *25*–*28*). However, the rapid death of HIV-1–infected cells has made it difficult to establish that antibodies can accelerate the clearance of infected cells in vivo. Our mathematical analysis of patient data, and the antibody-mediated reduction in infected cells seen in adoptive transfer experiments, establish that bNAbs alter the half-life of infected cells. This observation may help explain why postexposure prophylaxis with bNAbs is more effective than ART in hu-mice (*23*).

Experiments with human cells in mice cannot fully recapitulate the human host; nevertheless, these experiments establish that antibodies can accelerate clearance of infected cells in vivo and do so by an FcγR-dependent mechanism. The finding that antibodies can clear infected cells in vivo has important implications for therapies aimed at HIV prevention and viral reservoir reduction or elimination.

REFERENCES AND NOTES

1. H. Mouquet, *Trends Immunol.* **35**, 549–561 (2014).
2. A. P. West Jr. *et al.*, *Cell* **156**, 633–648 (2014).
3. M. Caskey *et al.*, *Nature* **522**, 487–491 (2015).
4. T. Igarashi *et al.*, *Nat. Med.* **5**, 211–216 (1999).
5. M. Kramski, M. S. Parsons, I. Stratov, S. J. Kent, *Curr. HIV Res.* **11**, 388–406 (2013).
6. Z. Euler, G. Alter, *AIDS Res. Hum. Retroviruses* **31**, 13–24 (2015).
7. G. Doitsh *et al.*, *Nature* **505**, 509–514 (2014).
8. A. S. Perelson *et al.*, *Nature* **387**, 188–191 (1997).
9. V. Müller, A. F. Marée, R. J. De Boer, *J. Virol.* **75**, 2597–2603 (2001).
10. R. J. De Boer, R. M. Ribeiro, A. S. Perelson, *PLOS Comput. Biol.* **6**, e1000906 (2010).
11. Supplementary analysis is available as supplementary materials on *Science* Online.
12. B. Joos *et al.*, *Antimicrob. Agents Chemother.* **50**, 1773–1779 (2006).
13. P. D. Gibaldi M, *Pharmacokinetics* (Marcel Dekker, New York, ed. 2, 1982).
14. G. Fätkenheuer *et al.*, *Nat. Med.* **11**, 1170–1172 (2005).
15. M. Kramski, I. Stratov, S. J. Kent, *AIDS* **29**, 137–144 (2015).
16. H. M. Horton *et al.*, *Blood* **116**, 3004–3012 (2010).
17. J. Pietzsch *et al.*, *Proc. Natl. Acad. Sci. U.S.A.* **109**, 15859–15864 (2012).
18. S. Bournazos *et al.*, *Cell* **158**, 1243–1253 (2014).
19. S. Bournazos, D. J. DiLillo, J. V. Ravetch, *J. Exp. Med.* **212**, 1361–1369 (2015).
20. P. Smith, D. J. DiLillo, S. Bournazos, F. Li, J. V. Ravetch, *Proc. Natl. Acad. Sci. U.S.A.* **109**, 6181–6186 (2012).
21. B. Su, C. Moog, *Front. Immunol.* **5**, 289 (2014).
22. A. J. Hessell *et al.*, *Nature* **449**, 101–104 (2007).
23. A. Halper-Stromberg *et al.*, *Cell* **158**, 989–999 (2014).
24. A. W. Boesch, E. P. Brown, M. E. Ackerman, *Immunol. Rev.* **268**, 296–310 (2015).
25. J. Pollara *et al.*, *Curr. HIV Res.* **11**, 378–387 (2013).
26. G. K. Lewis, *Immunology* **142**, 46–57 (2014).
27. J. R. Mascola, D. C. Montefiori, *Annu. Rev. Immunol.* **28**, 413–444 (2010).
28. B. F. Haynes *et al.*, *N. Engl. J. Med.* **366**, 1275–1286 (2012).

ACKNOWLEDGMENTS

We thank all study participants who devoted time to our research. We thank the Rockefeller University Hospital Clinical Research Support Office and nursing staff for patient care and recruitment. We thank T. Eisenreich for help with mouse colony management, K. Yao and S. Hinklein for technical help, P. Smith for FcγR humanized mice, CellDex Therapeutics for providing 3BNC117 and 10-1074, and all members of the Nussenzweig laboratory for helpful discussion and advice. The data reported in this paper are tabulated in the main paper and in the supplementary materials. This work was supported by Collaboration for AIDS Vaccine Discovery grant OPP1033115 (M.C.N. and J.V.R.). This work was also supported, in part, by grant 8 UL1 TR000043 from the National Center for Advancing Translational Sciences (NCATS); NIH Clinical and Translational Science Award (CTSA) program; NIH Center for HIV/AIDS Vaccine Immunology and Immunogen Discovery (CHAVI-ID) 1UM1 AI100663-01 (M.C.N); Bill and Melinda Gates Foundation grants OPP1092074 and OPP1124068 (M.C.N); the Robertson Foundation to M.C.N.; German Research Foundation postdoctoral fellowship SCHO 1612/1-1 (T.S.); NIH grant F31 AI118555-01 (J.A.H.); the American Foundation for AIDS research (amfAR) Mathilde Krim Fellowship in Basic Biomedical Research (108977-57-RKVA) (S.B.); the Ragon Institute of Massachusetts General Hospital, Massachusetts Institute of Technology, and Harvard (A.K.C.); a NSF Graduate Research Fellowship under grant no. 1122374 (D.K.M.); and National Institute of Allergy and Infectious Diseases (NIH) grants AI100148-02 and AI081677-05 (M.C.N. and J.V.R.). The content is solely the responsibility of the authors and does not necessarily represent the official views of the NIH. M.C.N. is a Howard Hughes Medical Institute Investigator. There are pending patent applications on the 3BNC117 and 10-1074 antibodies by Rockefeller University on which M.C.N. is an inventor. The patents are not licensed by any companies.

SUPPLEMENTARY MATERIALS

www.sciencemag.org/content/352/6288/1001/suppl/DC1
Materials and Methods
Supplementary Text
Figs. S1 to S10
Tables S1 to S3
References (*29*–*37*)

21 December 2015; accepted 11 April 2016
Published online 5 May 2016
10.1126/science.aaf1279

DYNAMIC CYTOSKELETON

Accelerated actin filament polymerization from microtubule plus ends

Jessica L. Henty-Ridilla, Aneliya Rankova, Julian A. Eskin, Katelyn Kenny, Bruce L. Goode*

Microtubules (MTs) govern actin network remodeling in a wide range of biological processes, yet the mechanisms underlying this cytoskeletal cross-talk have remained obscure. We used single-molecule fluorescence microscopy to show that the MT plus-end–associated protein CLIP-170 binds tightly to formins to accelerate actin filament elongation. Furthermore, we observed mDia1 dimers and CLIP-170 dimers cotracking growing filament ends for several minutes. CLIP-170–mDia1 complexes promoted actin polymerization ~18 times faster than free–barbed-end growth while simultaneously enhancing protection from capping proteins. We used a MT-actin dynamics co-reconstitution system to observe CLIP-170–mDia1 complexes being recruited to growing MT ends by EB1. The complexes triggered rapid growth of actin filaments that remained attached to the MT surface. These activities of CLIP-170 were required in primary neurons for normal dendritic morphology. Thus, our results reveal a cellular mechanism whereby growing MT plus ends direct rapid actin assembly.

Tight coordination between the microtubule (MT) and actin cytoskeletons is required for fundamental processes such as directed cell migration, neuronal arborization, and phagocytosis (*1*–*3*). In many of these settings, the growth of MT plus ends into actin-rich cortical regions triggers changes in actin assembly–based functions (*4*, *5*). In plant cells, after washout of the actin depolymerizing drug latrunculin B, new actin polymerization occurs from MT plus ends (*6*). In fission yeast, MT plus ends direct formin-mediated actin cable assembly during "new end take off" (*7*, *8*). In other systems, MT plus ends play an instrumental role in steering actin-based motility of neuronal growth cones during neurite outgrowth and axonal guidance (*9*–*11*). Thus, it has long been hypothesized that molecular cues associated with MT plus ends directly govern

Department of Biology, Brandeis University, 415 South Street, Waltham, MA 02454, USA.
*Corresponding author. Email: goode@brandeis.edu

localized actin assembly; however, no such mechanism has been defined.

Formins directly stimulate both the nucleation and elongation phases of actin filament assembly, and they perform essential roles in constructing diverse cellular actin structures, including actin cables, stress fibers, filopodia, phagocytic cups, and cytokinetic rings (*3*). The dimeric formin homology 2 (FH2) domain nucleates actin filaments and remains processively attached to their growing barbed ends as they elongate, whereas the adjacent FH1 domains recruit profilin-bound actin monomers to accelerate elongation (*12*, *13*). The mammalian formin mDia1 supports one of the fastest known rates of actin filament elongation, at 55 subunits s^{-1} μM^{-1} (*13*).

CLIP-170 localizes to MT plus ends in cells via interactions with the MT end-binding protein EB1 but also localizes to actin-rich cortical zones (*5*, *14*–*19*). In addition, CLIP-170 binds and colocalizes with mDia1 in macrophages, where both proteins are required for phagocytosis (*5*), suggesting that their in vivo functions are tied together. The budding yeast protein Smy1 directly inhibits the yeast formin Bnr1, targeting its FH2 domain (*20*) via formin elongation effector domain (FEED) motifs (*21*). We discovered a FEED-like sequence in human CLIP-170, located in its central coiled-coil–rich region (Fig. 1A and fig. S1A). Thus, we purified full-length human CLIP-170 and used total internal reflection fluorescence (TIRF) microscopy to test its possible effects on mDia1-mediated actin assembly.

Mammalian CLIP-170 is expressed as three alternatively spliced isoforms (CLIP-170-1, CLIP-170-2, and CLIP-170-3) (fig. S1A). All splicing occurs in a specific region of CLIP-170 [amino acids (aa) 457 to 502], and the FEED motif, which is present in all three isoforms, borders the spliced region (fig. S1A). We purified all three isoforms of CLIP-170 as full-length proteins and tested their effects on mDia1 (FH1-FH2-tail)–mediated actin assembly. The CLIP-170 isoforms had no effect on actin assembly alone, but each one substantially accelerated the rate of mDia1-mediated actin filament elongation (Fig. 1, B to E; fig. S1, B to E; and movies S1 and S2). In constrast, these isoforms showed statistically insignificant effects on formin-mediated actin nucleation (fig. S1F). A closer examination of the distribution of filament elongation rates in reactions containing both mDia1 and CLIP-170 revealed three subpopulations with distinct rates (Fig. 1E and movie S2). The slowest had a mean elongation rate of 10.1 ± 1.3 (SE) subunits s^{-1} μM^{-1}, similar to the rate of free–barbed-end growth (*22*). The second subpopulation had a faster rate of 58.8 ± 8.8 subunits s^{-1} μM^{-1}, similar to filament elongation mediated by mDia1 alone (Fig. 1E and movie S2). The third was substantially accelerated, elongating at 179.1 ± 39.1 subunits s^{-1} μM^{-1}, or ~18 times faster than free–barbed-end growth in the absence of formins. This accelerated elongation occurred exclusively in reactions containing mDia1 and CLIP-170 and was observed at different actin concentrations (fig. S2). The fraction of filaments in the reaction undergoing accelerated elongation scaled with increasing concentrations of CLIP-170 (Fig. 1E). Because 25 nM CLIP-170 supported the strongest effects, this concentration was used for all further tests. CLIP-170 also increased the elongation rates of filaments assembled by four other formins (mDia2, Daam1, INF1, and INF2) (Fig. 1F and fig. S3). Thus, the regulatory effects of CLIP-170 extend to multiple formins, not just mDia1.

Accelerated elongation required profilin and the FH1 and FH2 domains of mDia1 (Fig. 1G). These are precisely the same requirements for mDia1-accelerated elongation without CLIP-170 (Fig. 1G)

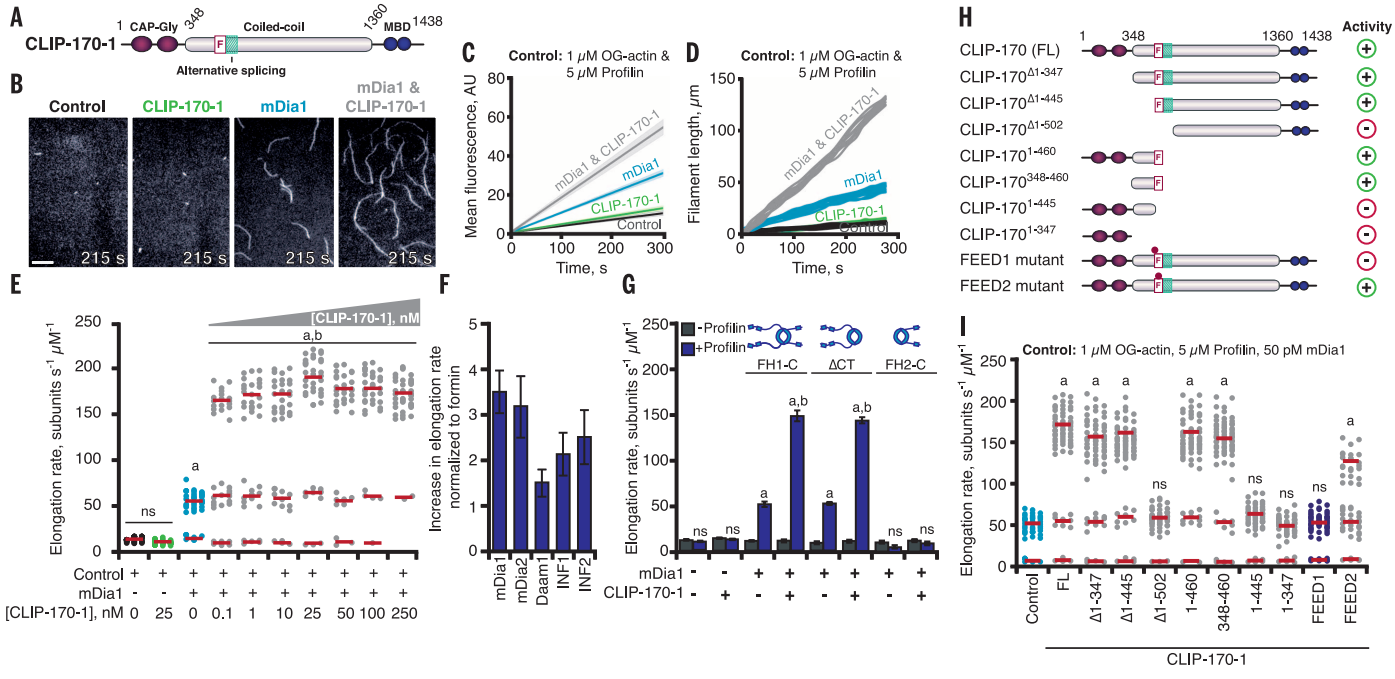

Fig. 1. CLIP-170 accelerates formin-mediated actin filament elongation. (**A**) CLIP-170 domains. F, FEED sequence; MBD, metal-binding domain. (**B**) Images from TIRF assays containing 50 pM mDia1 and/or 25 nM CLIP-170-1, taken 215 s after initiation of actin assembly. Scale bar, 20 μm. (**C**) Kinetics of total actin polymer mass (fluorescence intensity) accumulation averaged from multiple ($n \geq 3$) fields of view. Linear fits plotted with 95% confidence intervals are shown as shaded areas. AU, arbitrary units; OG-actin, Oregon Green actin. (**D**) Representative filament length traces (10 per condition) from TIRF movies. (**E**) Distributions of elongation rates from TIRF reactions, as in (B), for different concentrations of CLIP-170-1. Distributions are shown from one of three independent experiments (n = 50 filaments each). The red bars show mean elongation rates for subpopulations, measured from all filaments in three separate experiments (n = 150 filaments). (**F**) Fold increase in mean formin-mediated elongation rate stimulated by 25 nM CLIP-170-1. Error bars indicate SE. (**G**) Mean elongation rates from TIRF reactions containing different mDia1 constructs with or without profilin. (**H**) CLIP-170-1 constructs that enhance (+) or fail to enhance (–) the rate of mDia1-mediated elongation. FL, full length; F, FEED sequence; teal box, alternatively spliced region; red dots, FEED1 [^{445}VEEE/AAAA^{448} (V, Val; E, Glu; A, Ala)] and FEED2 [^{450}ITKGDLE/AAAAAAA^{456} (I, Ile; T, Thr; K, Lys; G, Gly; D, Asp; L, Leu)] mutants. (**I**) Distributions of elongation rates measured as in (E) for different CLIP-170-1 constructs. Reactions contained 1 μM globular actin (G-actin) (10% OG-labeled; 0.2% biotin-actin), ± 5 μM profilin, ± 50 pM mDia1, 50 pM mDia2, 50 pM Daam1, 100 nM INF1 or 100 nM INF2, ± 25 nM full-length CLIP-170-1 (WT, FEED1 mutant, or FEED2 mutant). Statistical differences in (E), (G), and (I): ns, not significantly different from control; a, compared with control (actin and profilin) ($P < 0.05$); b, compared with formin control (actin, profilin, and formin) ($P < 0.05$).

(*13*, *23*). Thus, CLIP-170 may be functioning by further improving the mechanism of elongation that is already used by formins. We mapped the activities in CLIP-170 to specific domains (Fig. 1, H and I). Because all three CLIP-170 isoforms had similar effects on mDia1, we mapped activities in the longest isoform, CLIP-170-1. All CLIP-170-1 fragments containing the FEED sequence supported accelerated elongation, and a short fragment (aa 348 to 460) encompassing the FEED sequence was sufficient, whereas the N-terminal MT- and EB1-binding region (aa 1 to 347) (*15*) was dispensable. Next, we generated two mutant alleles (alanine substitutions) in the FEED sequence of full-length CLIP-170-1 (fig. S1A). The FEED1 mutant abolished accelerated elongation, and the FEED2 mutant reduced the rate of accelerated elongation (Fig. 1I). Thus, CLIP-170–mediated effects on mDia1 are FEED-dependent.

A number of possible mechanisms could explain the effects of CLIP-170 on mDia1, including formation of stable or transient CLIP-170–mDia1 complexes at growing barbed ends of filaments. To address this, we used multiwavelength single-molecule TIRF microscopy to directly observe fluorescently labeled SNAP-tagged CLIP-170-1 and mDia1 molecules interacting with actin filaments during their assembly. 649-mDia1 and untagged mDia1 are dimeric and have indistinguishable activities (*24*). Step photobleaching analysis showed that 549-CLIP-170-1 molecules were also predominantly dimers (fig. S4), as expected (*15*). 649-mDia1 molecules processively tracked the barbed ends of filaments (Fig. 2A and movie S3, left panel) (*24*), and 549-CLIP-170-1 showed rare interactions with filaments. However, in reactions containing both 649-mDia1 and 549-CLIP-170-1, these proteins tracked the growing barbed end together (Fig. 2, A to E, and movie S3, right panel). 549-CLIP-170-1 and untagged CLIP-170-1 stimulated indistinguishable rates of formin-dependent accelerated elongation (Fig. 2B).

Accelerated elongation occurred only when 649-mDia1 and 549-CLIP-170-1 were observed together at the barbed end (300 out of 300 events) (Fig. 2, B to E, and movie S4). In our 3-min observation window, CLIP-170–dissociation events were rare (only 2 out of 100 barbed ends tracked), which suggests that CLIP-170-1–mDia1 barbed-end tracking complexes are long-lived and highly processive. In a few instances, we observed formation and dissolution of the mDia1–CLIP-170 complex (Fig. 2, D and E). The filament shown initially grew at the free–barbed-end rate (with no mDia1 or CLIP-170-1 associated); upon association of 649-mDia1, growth transitioned to a faster rate; and, subsequently, when 549-CLIP-170-1 joined the formin on the barbed end, growth immediately jumped to the further-enhanced rate. After several minutes, 549-CLIP-170-1 dissociated, and growth fell back to the mDia1-supported rate. When 649-mDia1 dissociated, growth returned to the free–barbed-end rate. Thus, when CLIP-170 joins mDia1 at the filament end, it forms a processive barbed-end tracking complex that enhances elongation. Single-molecule experiments also showed that CLIP-170-1 binds anchored mDia1, even in the absence of actin, and that binding is competitively displaced by an excess CLIP-170-1 fragment (aa 348 to 460) (Fig. 2F).

A hallmark of formins is their ability to protect growing barbed ends from capping protein

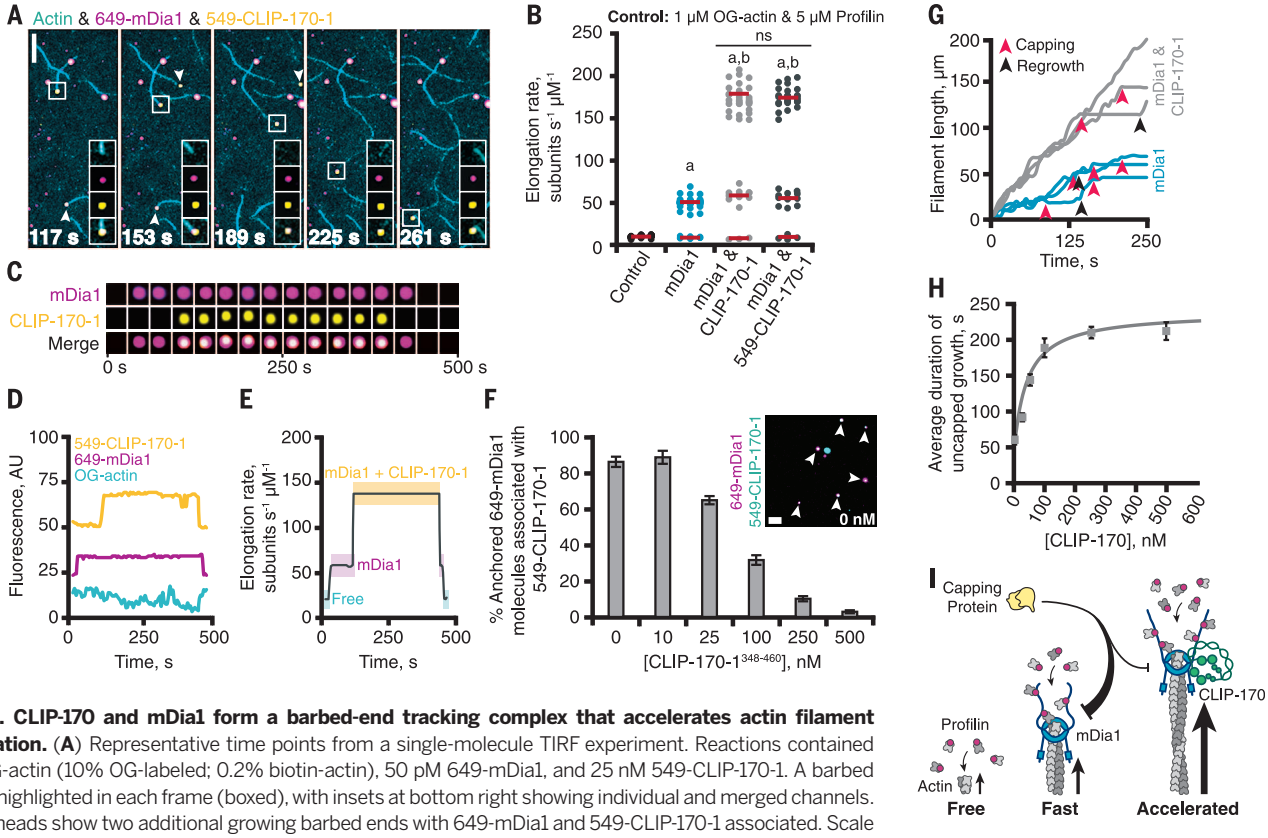

Fig. 2. CLIP-170 and mDia1 form a barbed-end tracking complex that accelerates actin filament elongation. (**A**) Representative time points from a single-molecule TIRF experiment. Reactions contained 1 μM G-actin (10% OG-labeled; 0.2% biotin-actin), 50 pM 649-mDia1, and 25 nM 549-CLIP-170-1. A barbed end is highlighted in each frame (boxed), with insets at bottom right showing individual and merged channels. Arrowheads show two additional growing barbed ends with 649-mDia1 and 549-CLIP-170-1 associated. Scale bar, 10 μm. Insets, 5 μm by 5 μm. (**B**) Effects of 25 nM CLIP-170-1 or 549-CLIP-170-1 on the rate of mDia1-mediated actin filament elongation. Reactions were as described in (A). Statistical differences: ns, not significantly different from control; a, compared with control (actin and profilin) ($P < 0.05$); b, compared with formin control (actin, profilin, and formin) ($P < 0.05$). (**C**) Formation and dissociation of a CLIP-170–mDia1 complex at a barbed end. (**D**) Fluorescence intensity profiles for each channel, showing formation and dissociation of the CLIP-170–mDia1 complex in (C). (**E**) Elongation rates correlate with arrival and dissociation of mDia1 and/or CLIP-170 at the barbed end. (**F**) Single-molecule colocalization of anchored 649-mDia1 and soluble full-length 549-CLIP-170-1 at different concentrations of unlabeled competitor fragment CLIP-170-1$^{348-460}$. Data were averaged from three fields of view in each of three independent experiments. Error bars indicate SE. The inset shows a representative field of view from a reaction with no competitor. Scale bar, 5 μm. (**G**) Representative filament traces from TIRF movies, conditions as in (A) except for the addition of 3 nM CP. Capping events (red arrowheads) and regrowth events (black arrowheads) are highlighted. (**H**) CLIP-170-1 enhances the duration of mDia1-mediated elongation in the presence of CP. Error bars indicate SE. (**I**) Cartoon of CLIP-170 joining mDia1 at the barbed end and increasing the rate of elongation and duration of growth in the presence of CP.

(CP) (*25*–*27*). To test whether CLIP-170 influences this function of mDia1 (*26*, *28*), we spiked in different concentrations of CP early in bulk assays. CP slowed mDia1-mediated actin assembly in a dose-dependent manner (fig. S5A). These results are consistent with recent studies showing that CP and mDia1 can simultaneously interact with barbed ends and each catalyze dissociation of the other (*29*, *30*). CLIP-170-1 attenuated the effects

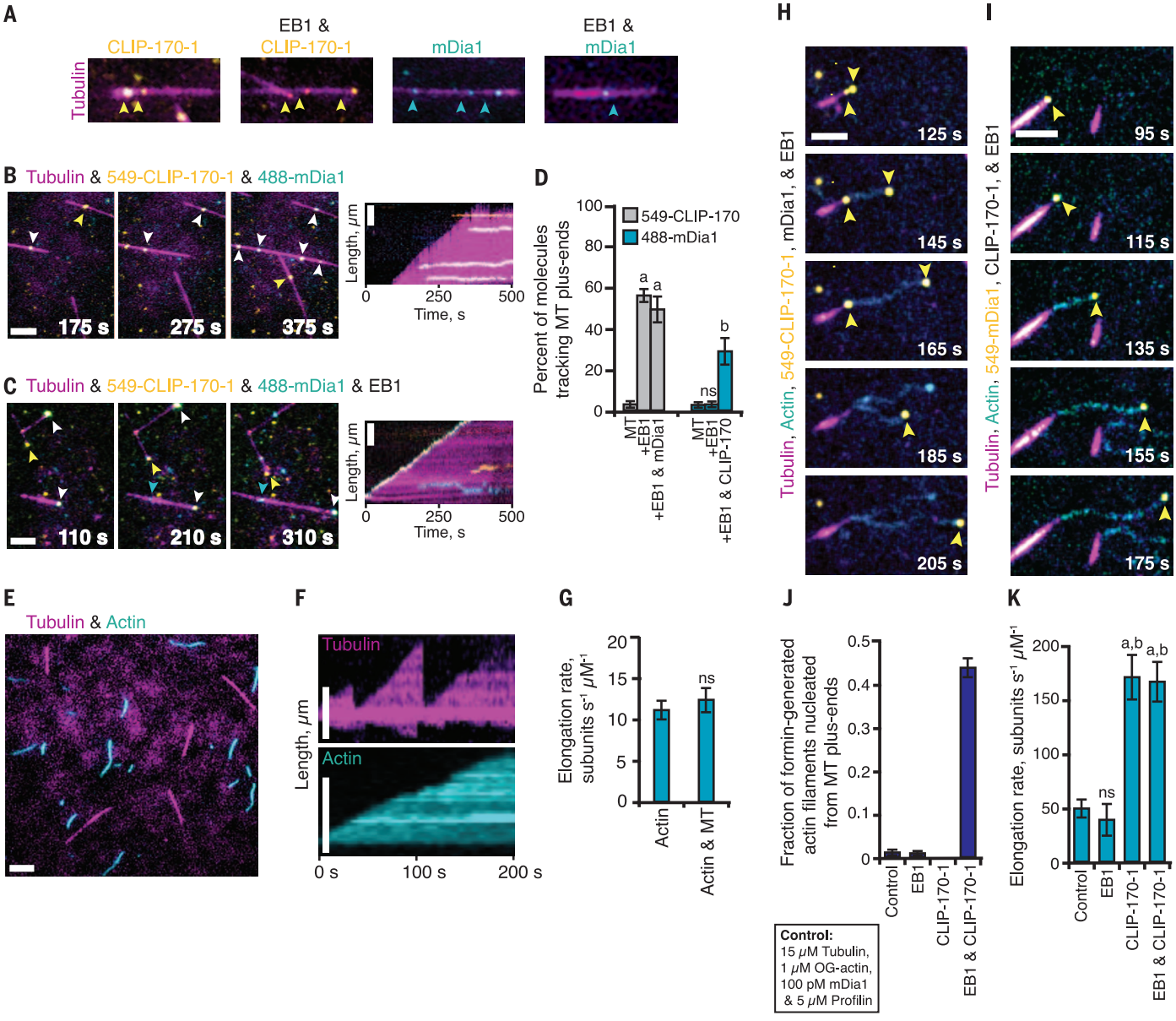

Fig. 3. CLIP-170–mDia1 complexes are recruited to MT plus ends by EB1 and stimulate actin polymerization from the MT surface. (**A**) TIRF movies show that 549-CLIP-170-1 binds MT sides and tracks MT plus ends only in the presence of EB1 (*17*). 488-mDia1 binds MT sides, with or without EB1, and does not track MT plus ends. Yellow arrowheads indicate CLIP-170 molecules; blue arrowheads indicate mDia1 molecules. (**B** and **C**) 549-CLIP-170-1 and 488-mDia1 colocalize on MT sides (B) and track MT plus ends together specifically in the presence of EB1 (C). White arrowheads indicate the presence of both CLIP-170 and mDia1 on MT plus ends. Scale bars, 5 μm. Reactions in (A) to (C) contain 15 μM tubulin (30% AlexaFluor649-labeled), biotinylated guanosine monophosphate–CPP MT seeds, and variable components (25 nM 549-CLIP-170-1, 100 pM 488-mDia1, and 500 nM EB1). (**D**) Percentage of molecules tracking MT plus ends from reactions in (A) to (C). Data were averaged from three experiments ($n > 100$ molecules). Statistical differences: ns, not different from control; a, compared with CLIP-170-1 ($P < 0.05$); b, compared with mDia1 ($P < 0.05$). (**E**) Co-reconstitution of MTs undergoing dynamic instability and polymerization of actin filaments. Reactions contained all of the same components as in (A) to (C), plus 1 μM G-actin (10% OG-labeled; 0.2% biotin-actin) and 5 μM profilin. Scale bar, 5 μm. (**F**) Kymographs of MT and actin dynamics. Scale bars, 5 μm. (**G**) The rate of actin filament elongation does not change significantly in the presence and absence of MTs. Data were averaged from three experiments ($n = 50$ actin filaments). (**H**) With the addition of unlabeled EB1 and mDia1, 549-CLIP-170-1 molecules (yellow arrowheads) were recruited to MT plus ends, where they triggered assembly of actin filaments that grew at the accelerated rate. Scale bar, 5 μm. (**I**) Similar observations as in (H), except using 549-mDia1 and unlabeled CLIP-170-1. Note that, in this panel, the yellow arrowheads indicate 549-mDia1 (rather than CLIP-170). Scale bar, 5 μm. (**J**) Fraction of formin-generated actin filaments that grew from MT plus ends in reactions as in (H) and (I). Data were from three experiments ($n = 50$ filaments per condition). (**K**) Actin elongation rates from reactions as in (H) and (I). Data were from three experiments ($n = 50$ filaments per condition). Statistical differences: ns, not different from control; a, compared with actin alone or control ($P < 0.05$); b, compared with EB1 control ($P < 0.05$). Error bars in (D) and (G) to (K), SE.

of CP on mDia1 in these assays (fig. S5B). In TIRF microscopy assays, CLIP-170-1 increased the average elongation rate of mDia1-nucleated filaments in the presence of CP (fig. S5C). Similar effects were observed for each CLIP-170-1 construct that supported accelerated elongation (fig. S5D). CLIP-170-1 also increased the duration of accelerated growth in the presence of CP (Fig. 2, G and H, and fig. S5C) by up to a factor of 4. CP effects were sometimes reversed, as indicated by an abrupt return to growth at mDia1-supported rates, but these events were rare (n < 10 occurrences for each condition out of 300 capping events analyzed). On the other hand, CLIP-170 did not significantly affect the average duration of capping before growth resumed (fig. S5E). Thus, not only does CLIP-170 increase the rate of mDia1-mediated actin filament elongation by a factor of 3 to 4, it also prompts a fourfold increase in growth duration in the presence of CP (Fig. 2I).

CLIP-170 and mDia1 each bind MTs and EB1 (*17*, *31*–*34*). We thus investigated CLIP-170 and mDia1 interactions, alone and together, with dynamic MTs in the presence and absence of EB1 (Fig. 3A). 549-CLIP-170-1 interacted with MT sides and was recruited to growing MT ends by EB1 (Fig. 3A; fig. S6, A and B; and movie S5), as expected (*17*). 488-mDia1 bound to MT sides, both in the presence and absence of EB1, but was not recruited to MT ends (Fig. 3A; fig. S6, C and D; and movie S6). In the absence of EB1, 488-mDia1 colocalized with 549-CLIP-170-1 on MT sides (Fig. 3B and movie S6). However, in the presence of both EB1 and 549-CLIP-170-1, 488-mDia1 was recruited to the MT plus ends (Fig. 3C and movie S6). These observations demonstrate a hierarchal recruitment scheme wherein EB1 recruits CLIP-170, which recruits mDia1 to growing MT ends.

We developed a co-reconstitution TIRF system that enabled imaging of MTs undergoing dynamic instability and actin filaments polymerizing simultaneously (Fig. 3, E to G, and movie S7). In the presence of EB1, CLIP-170, and mDia1 (but not in reactions lacking any of these components), we observed coordination of growing MT ends with formation of rapidly polymerizing actin filaments. With unlabeled EB1 and mDia1, 549-CLIP-170-1 molecules were dynamically recruited to growing MT plus ends, where they triggered formation of actin filaments that polymerized from the MT surface (Fig. 3H and movie S8). Similar observations were made with unlabeled EB1, unlabeled CLIP-170-1, and 549-mDia1 (Fig. 3I and movie S9). About half of the actin filaments assembled by mDia1 originated from MT plus ends (Fig. 3J); in each case, 549-CLIP-170-1 or 549-mDia1 tracked the growing barbed ends, which polymerized at the accelerated rate away from the MT (Fig. 3K). Actin filament pointed ends remained attached to the MT surface for 45 ± 10.3 s, on average, until they spontaneously detached or were released by a MT catastrophe event.

To test the importance of these activities in a more physiological setting, we used a short hairpin RNA (shCLIP-170) to interfere with expression of all three CLIP-170 isoforms in rat primary cortical neurons (Fig. 4, A and B). Dendritic elaboration in these neurons depends on tight coordination between the MT and actin cytoskeletons (*11*, *16*, *35*). Depletion of CLIP-170 (validated in N2A cells; fig. S7) led to markedly reduced complexity of neuronal processes, as previously reported (*16*). This phenotype was rescued by a full-length wild-type (WT) CLIP-170-1 construct resistant to silencing (Fig. 4, A and B), but not the FEED1 mutant (Fig. 4,

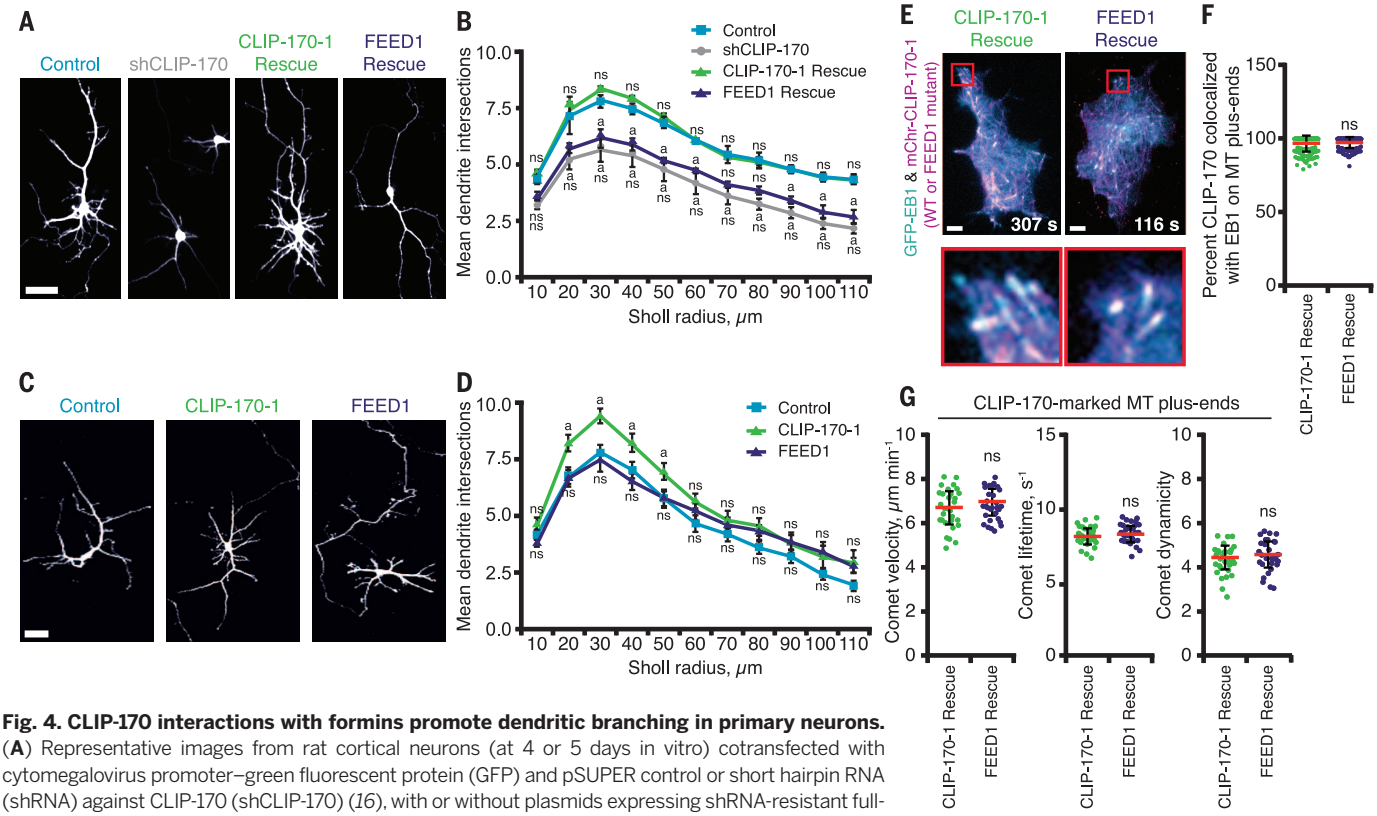

Fig. 4. CLIP-170 interactions with formins promote dendritic branching in primary neurons. (**A**) Representative images from rat cortical neurons (at 4 or 5 days in vitro) cotransfected with cytomegalovirus promoter–green fluorescent protein (GFP) and pSUPER control or short hairpin RNA (shRNA) against CLIP-170 (shCLIP-170) (*16*), with or without plasmids expressing shRNA-resistant full-length CLIP-170-1 rescue (WT or FEED1 mutant). Scale bar, 5 μm. (**B**) Quantification of dendritic branching complexity by Sholl analysis (n = 90 to 120 neurons, from two or more independent experiments). Statistical differences: ns, not significantly different from control; a, compared with scramble shRNA control (P < 0.05). There was never a significant difference between the FEED1 rescue and the shCLIP-170 knockdown alone. Error bars indicate SE. (**C**) Representative images from rat cortical neurons, as in (A), expressing full-length CLIP-170-1 (WT or FEED1 mutant) without silencing endogenous CLIP-170. Scale bar, 5 μm. (**D**) Quantification of dendritic branching complexity by Sholl analysis as in (B), except data are from n = 60 neurons in two independent experiments. Statistical differences: ns, not significantly different from control; a, compared with scramble shRNA control (P < 0.05). Error bars indicate SE. (**E**) Localization of mCherry–CLIP-170-1 (WT or FEED1 mutant) rescue constructs in N2A cells in which endogenous CLIP-170 was silenced. Scale bars, 10 μm. (**F**) Quantification of mCherry–CLIP-170-1 colocalization with EB1-GFP at MT plus ends from cells as in (E). Error bars indicate SD. (**G**) Quantitative tracking of mCherry–CLIP-170-1 (WT or FEED1 mutant) comets on growing MT plus ends. Analysis included comet velocity (or MT growth rate), comet lifetime (MT growth duration), and comet "dynamicity" [a general readout of MT dynamics (*37*)]. Error bars indicate SD.

A and B). Conversely, increased expression of WT CLIP-170-1 over endogenous CLIP-170 led to elevated dendritic complexity, as previously shown (*16*), whereas expression of mutant CLIP-170-1 did not (Fig. 4, C and D). In N2A cells, WT and FEED1 mutant CLIP-170-1 were expressed at similar levels (fig. S7). Live imaging showed that they localized to MT plus ends similarly (Fig. 4, E and F; fig. S8, A to C; and movie S10) and that the mutant did not alter MT dynamics (Fig. 4G; fig. S8, D and E; and movies S10 and S11). Thus, CLIP-170 interactions with formins play an important role in coordinating MT and actin dynamics to regulate neuronal process formation.

Here we have shown that CLIP-170 interacts tightly with formins to substantially increase both the rate of actin filament elongation and the duration of elongation in the presence of CP. CLIP-170 is part of a mechanism that enables growing MT plus ends to trigger rapid assembly of actin filaments in vitro, directly linking MT and actin dynamics. This mechanism was consistent in a physiological setting, where EB1 and CLIP-170 colocalized on MT plus ends, as well as with previous reports that growing MT plus ends survey the actin-rich cortex (*10*) and that ~10% of mDia1 puncta in cells colocalize with MT plus ends (*32*). In neurons, CLIP-170 interactions with formins were required for proper dendritic branching. Similar mechanisms may explain the colocalization and cofunctioning of CLIP-170 and mDia1 in phagocytic cup formation (*5*) and reduced actin-based protrusive activity in neuronal growth cones after CLIP-170 silencing (*18*, *19*, *35*, *36*).

REFERENCES AND NOTES

1. P. Forscher, S. J. Smith, *J. Cell Biol.* **107**, 1505–1516 (1988).
2. O. C. Rodriguez *et al.*, *Nat. Cell Biol.* **5**, 599–609 (2003).
3. M. A. Chesarone, A. G. DuPage, B. L. Goode, *Nat. Rev. Mol. Cell Biol.* **11**, 62–74 (2010).
4. T. M. Svitkina *et al.*, *J. Cell Biol.* **160**, 409–421 (2003).
5. E. Lewkowicz *et al.*, *J. Cell Biol.* **183**, 1287–1298 (2008).
6. A. Sampathkumar *et al.*, *Plant Cell* **23**, 2302–2313 (2011).
7. S. G. Martin, W. H. McDonald, J. R. Yates III, F. Chang, *Dev. Cell* **8**, 479–491 (2005).
8. S. G. Martin, S. A. Rincón, R. Basu, P. Pérez, F. Chang, *Mol. Biol. Cell* **18**, 4155–4167 (2007).
9. D. M. Suter, P. Forscher, *J. Neurobiol.* **44**, 97–113 (2000).
10. W. C. Salmon, M. C. Adams, C. M. Waterman-Storer, *J. Cell Biol.* **158**, 31–37 (2002).
11. C. H. Coles, F. Bradke, *Curr. Biol.* **25**, R677–R691 (2015).
12. M. Chesarone, C. J. Gould, J. B. Moseley, B. L. Goode, *Dev. Cell* **16**, 292–302 (2009).
13. D. R. Kovar, E. S. Harris, R. Mahaffy, H. N. Higgs, T. D. Pollard, *Cell* **124**, 423–435 (2006).
14. A. Akhmanova *et al.*, *Cell* **104**, 923–935 (2001).
15. K. C. Slep, R. D. Vale, *Mol. Cell* **27**, 976–991 (2007).
16. D. Neukirchen, F. Bradke, *J. Neurosci.* **31**, 1528–1538 (2011).
17. R. Dixit *et al.*, *Proc. Natl. Acad. Sci. U.S.A.* **106**, 492–497 (2009).
18. J.-H. Weng *et al.*, *Nat. Chem. Biol.* **9**, 636–642 (2013).
19. R. Beaven *et al.*, *Mol. Biol. Cell* **26**, 1491–1508 (2015).
20. M. Chesarone-Cataldo *et al.*, *Dev. Cell* **21**, 217–230 (2011).
21. J. A. Eskin, A. Rankova, A. B. Johnston, S. L. Alioto, B. L. Goode, *Mol. Biol. Cell* **27**, 828–837 (2016).
22. J. R. Kuhn, T. D. Pollard, *Biophys. J.* **88**, 1387–1402 (2005).
23. C. J. Gould *et al.*, *Curr. Biol.* **21**, 384–390 (2011).
24. D. Breitsprecher *et al.*, *Science* **336**, 1164–1168 (2012).
25. J. B. Moseley *et al.*, *Mol. Biol. Cell* **15**, 896–907 (2004).
26. S. H. Zigmond *et al.*, *Curr. Biol.* **13**, 1820–1823 (2003).
27. E. S. Harris, F. Li, H. N. Higgs, *J. Biol. Chem.* **279**, 20076–20087 (2004).
28. M. A. Wear, J. A. Cooper, *Trends Biochem. Sci.* **29**, 418–428 (2004).
29. J. P. Bombardier *et al.*, *Nat. Commun.* **6**, 8707 (2015).
30. S. Shekhar *et al.*, *Nat. Commun.* **6**, 8730 (2015).
31. P. Pierre, J. Scheel, J. E. Rickard, T. E. Kreis, *Cell* **70**, 887–900 (1992).
32. Y. Wen *et al.*, *Nat. Cell Biol.* **6**, 820–830 (2004).
33. J. Gaillard *et al.*, *Mol. Biol. Cell* **22**, 4575–4587 (2011).
34. F. Bartolini *et al.*, *J. Cell Biol.* **181**, 523–536 (2008).
35. L. Swiech *et al.*, *J. Neurosci.* **31**, 4555–4568 (2011).
36. C. Erck *et al.*, *Proc. Natl. Acad. Sci. U.S.A.* **102**, 7853–7858 (2005).
37. K. T. Applegate *et al.*, *J. Struct. Biol.* **176**, 168–184 (2011).

ACKNOWLEDGMENTS

We thank S. Paradis for guidance on experiments using neurons, D. Breitsprecher for pioneering the MT-actin co-reconstitution system, J. Gelles for guidance on single-molecule analysis, S. Jansen for guidance with cell culture, H. Higgs for providing INF1 and INF2 proteins, and L. Cassimeris for providing pGFP-EB1. This research was supported by NIH grant GM083137 to B.L.G. and Brandeis NSF Materials Research Science and Engineering Center grant 142038. J.L.H.-R. was supported in part by a fellowship from the Leukemia and Lymphoma Society and in part by NIH training grant T32NS007292. J.L.H.-R. and B.L.G. designed the experiments and wrote the manuscript, J.L.H.-R. performed the experiments and data analysis, J.A.E. performed data analysis, A.R. built reagents and performed preliminary experiments, and K.K. performed overexpression analysis in neurons and assisted in other neuronal work. We declare no conflicts of interest. The supplementary materials contain additional data.

SUPPLEMENTARY MATERIALS

www.sciencemag.org/content/352/6288/1004/suppl/DC1
Materials and Methods
Figs. S1 to S9
References (*38*–*48*)
Movies S1 to S11

29 December 2015; accepted 5 April 2016
10.1126/science.aaf1709

GENE EVOLUTION

Coregulation of tandem duplicate genes slows evolution of subfunctionalization in mammals

Xun Lan[1,3]* and Jonathan K. Pritchard[1,2,3]*

Gene duplication is a fundamental process in genome evolution. However, most young duplicates are degraded by loss-of-function mutations, and the factors that allow some duplicate pairs to survive long-term remain controversial. One class of models to explain duplicate retention invokes sub- or neofunctionalization, whereas others focus on sharing of gene dosage. RNA-sequencing data from 46 human and 26 mouse tissues indicate that subfunctionalization of expression evolves slowly and is rare among duplicates that arose within the placental mammals, possibly because tandem duplicates are coregulated by shared genomic elements. Instead, consistent with the dosage-sharing hypothesis, most young duplicates are down-regulated to match expression levels of single-copy genes. Thus, dosage sharing of expression allows for the initial survival of mammalian duplicates, followed by slower functional adaptation enabling long-term preservation.

Gene duplications are a major source of new genes and ultimately of new biological functions (*1*). However, recently arisen gene duplicates tend to be functionally redundant and thus susceptible to loss-of-function mutations that degrade one of the copies into a pseudogene. The average half-life of new primate duplicates has been estimated at just 4 million years (*2*). This raises the question of what evolutionary forces govern the persistence of young duplicates.

Various models have been proposed to understand why some duplicate pairs do survive over long evolutionary time scales (*3*). Dosage-balance models focus on the importance of maintaining correct stoichiometric ratios in gene expression between different genes (*4*–*6*) and likely explain how gene copies are maintained after whole-genome duplication (WGD), because subsequent gene losses would disrupt dosage balance (*6*, *7*).

Alternatively, functional partitioning of duplicates can occur, either by neofunctionalization (one copy gains new functions) or subfunctionalization (the copies divide the ancestral functions between them). The duplication-degeneration-complementation (DDC) model proposes that complementary degeneration of regulatory elements causes the two copies to be expressed in different tissues, such that both copies are required to provide the overall expression of the ancestral gene (*8*). Similarly, neofunctionalization of expression could lead to one gene copy gaining function in a tissue where the parent gene was not expressed. Functional divergence may also occur at the protein level (*9*), but this is thought to be a slow process, with initial divergence more often occurring through changes in gene regulation (*10*).

It is currently unclear which factors are most important for long-term survival of gene duplications in mammals, where most duplications arise

[1]Department of Genetics, Stanford University, Stanford, CA, USA. [2]Department of Biology, Stanford University, Stanford, CA, USA. [3]Howard Hughes Medical Institute, Stanford University, Stanford, CA, USA.
***Corresponding author. Email: xlan@stanford.edu (X.L.); pritch@stanford.edu (J.K.P.)**

Accelerated actin filament polymerization from microtubule plus ends

Jessica L. Henty-Ridilla, Aneliya Rankova, Julian A. Eskin, Katelyn Kenny and Bruce L. Goode

Science **352** (6288), 1004-1009.
DOI: 10.1126/science.aaf1709

Making the fast faster still

Coordination between actin and microtubule cytoskeleton dynamics is critical during cell migration, phagocytosis, cytokinesis, and embryogenesis. However, the basis for cross-regulation of cytoskeleton dynamics is unclear. Henty-Ridilla *et al.* found that a component of the microtubule cytoskeleton accelerates actin filament elongation and protects the growing actin filament end (see the Perspective by Rottner). Thus, growing microtubules appear to be able to directly control the actin assembly machinery and actin filament dynamics.

Science, this issue p. 1004; see also p. 894